

Magnetic domain structures in submicron-size particles of epitaxial Fe (001) films: Shape anisotropy and thickness dependence

M. Hanson* and O. Kazakova

Department of Solid State Physics, Chalmers University of Technology and Göteborg University, SE-412 96 Göteborg, Sweden

P. Blomqvist and R. Wäppling

Department of Physics, Uppsala University, Box 530, SE-751 21 Uppsala, Sweden

B. Nilsson

Microtechnology Center at Chalmers Process Laboratory, SE-412 96 Göteborg, Sweden

(Received 1 February 2002; published 30 October 2002)

In this work the influence of shape anisotropy on the magnetic hysteresis and zero-field magnetic domain state of submicron-size particles of Fe was investigated. Arrays of particles having circular (diameter $d_c = 550$ or 200 nm), rectangular (900 nm by 300 nm), or elliptical (450 nm by 150 nm) shape were prepared by electron lithography and ion-beam milling of epitaxial Fe (001) films of thicknesses $t=50, 30, 15,$ and 10 nm. The samples were characterized by magnetization measurements and magnetic-force microscopy (MFM). All films have cubic anisotropy, for $t=50, 30,$ and 15 nm with the same anisotropy constant as bulk Fe: $K_1 = (4.3 \pm 0.1) \times 10^4 \text{ J m}^{-3}$. For $t=10$ nm the effective anisotropy is increased, $K_1 = 5.7 \times 10^4 \text{ J m}^{-3}$, due to surface effects. The effects of the interplay between the magnetocrystalline and shape anisotropies are observed as the lateral extension of the films is decreased. The circular particles with $d_c = 550$ nm have closed magnetic domain structures with a fourfold symmetry, compatible with the magnetocrystalline anisotropy, for all thicknesses. In the rectangular particles a gradual change is observed as the thickness decreases. For $t=50$ nm a diamond structure comprising three closed-domain substructures is formed in the demagnetized state. The rectangles with $t=30$ and 15 nm are multidomains with the number of closed substructures decreasing to 2 and 1, respectively. The thickness dependence of the domain structure and an accompanying change of character in the MFM contrast are explained by an increasing amount of Néel component in the domain walls with a width that increases with decreasing film thickness. The rectangles with $t=10$ nm are quasingle domains, forming a flower state. The small circular particles ($d_c = 200$ nm) and the elliptical ones, both with $t=10$ nm, are considered to be stable single domains in zero field. Judging from the hysteresis curves, magnetization reversal does not occur by coherent rotation in any of the particles.

DOI: 10.1103/PhysRevB.66.144419

PACS number(s): 75.60.-d, 75.70.-i, 75.75.+a

I. INTRODUCTION

Modern techniques for film deposition and submicrometer patterning may be applied to prepare systems composed of arrays of small magnetic particles with well-defined geometric dimensions from films.¹ The study of such systems is in many cases motivated by their being possible candidates for applications, e.g., in high-density storage media² or as components in magnetoelectronic devices.^{3,4} Particle arrays, however, also comprise excellent model systems for studies of fundamental magnetic properties, since the shape and size of the particles as well as the distance between them can be varied independently of each other. The critical size for single-domain formation, the criteria for onset of interparticle interactions, and processes of magnetization reversal and magnetic relaxation may be studied. For this purpose the pure ferromagnetic elements Fe, Co, or Ni are better suited than multilayers or alloys, which would be chosen to meet the demands for specific applications, since the former are easier to prepare with reproducible intrinsic properties. In order to obtain an ensemble of particles of the best possible uniformity, it is also important to use epitaxial films, i.e., single-crystalline films with a fixed orientational relation to the substrate, as starting materials. With electron-beam li-

thography and ion-beam milling such particles, typically having lateral sizes in the range from 50 nm to $1 \mu\text{m}$, may be readily obtained. One particular task of interest is to find the size ranges where the transition between multidomain and single-domain particles occurs and to investigate the switching properties of such particles. There are earlier reports on studies of arrays of particles, with lateral extensions in the submicrometre range, made from epitaxial Fe,⁵⁻⁹ Co,¹⁰⁻¹³ and Ni.¹⁴ Of those three classical ferromagnets, on the whole, Co is the most extensively studied in films and patterned media. As was discussed in Ref. 13, single-domain particles were observed to form for film thicknesses of the order of 20 nm or below for about the same particle sizes in both epitaxial and polycrystalline Co films with in-plane magnetic anisotropy. Epitaxial films of Fe can be prepared and patterned to yield well-defined systems, in which the interplay between magnetocrystalline and shape anisotropies can be further studied. In an earlier work we prepared arrays of magnetic particles from 50 -nm-thick Fe (001) films.⁶ Those particles, circles with diameter $0.5 \mu\text{m}$ and rectangles, $0.3 \times 0.9 \mu\text{m}^2$, were multidomains comprising closed magnetic domain structures in zero field. The purpose of the present work is to investigate how the domain structure is affected when the shape anisotropy of such particles is

changed, by decreasing the film thickness and/or the lateral size of the Fe particles. In this paper we present magnetic hysteresis measurements and magnetic-force microscopy (MFM) images of two-dimensional arrays of particles prepared from epitaxial Fe (001) films of good quality. The film thicknesses range between 10 and 50 nm and the lateral sizes between 150 and 900 nm. Particles comprising single magnetic domains, which are stable in zero field, are found only for the thinnest film.

II. SAMPLE PREPARATION AND MAGNETIC CHARACTERIZATION

Epitaxial bcc Fe (001) films with thicknesses $t=10,15$, and 30 nm were grown as described earlier^{6,15} by magnetron sputtering on MgO (001) substrates, $10\times 10\times 0.5$ mm³. The samples were capped with a 2.5 nm layer of V, to prevent oxidation. The magnetic particles were prepared by a combination of electron-beam lithography and ion-beam milling, using a carbon masking layer and a NiCr layer serving as a transfer layer. The use of a hard carbon mask is a key step in our process making it possible to fabricate small particles with steep sidewalls and flat top surfaces from epitaxial films.⁶ Sets of particles with different sizes and repetition periods, covering areas 2×3 mm² of the 15- and 30-nm-thick films, were prepared. In the 10-nm-thick film the particles were positioned in blocks with 50×50 particles over regions 2.5×2.5 mm². For comparison we made additional measurements on the 50-nm-thick samples prepared for our earlier investigation.⁶ The particles were positioned in rectangular lattices with the axes along, or making an angle of 45° with, the (100) MgO directions, corresponding to the $\langle 110 \rangle$ and $\langle 100 \rangle$ directions in Fe. There is one set of samples for each of the two orientations in the 50-nm-thick film. For $t=30$ and 15 nm the films were patterned along the $\langle 110 \rangle$ directions and for $t=10$ nm along $\langle 100 \rangle$. Particles of circular shape with diameter $d_c=550$ nm and particles of rectangular shape having length $l=900$ nm and width $w=300$ nm were prepared for all film thicknesses. From the 10-nm-thick film also smaller particles were made: of circular shape with diameter $d_c=200$ nm and of elliptical shape having long and short axes $d_l=450$ nm and $d_s=150$ nm. In the 10-nm film the center-to-center distance between the rectangular particles is 1800 nm along the long and 1300 nm along the short axis and for the elliptical particles the corresponding distances are 900 and 1150 nm, respectively. In all other lattices the center-to-center distance between the particles is twice the particle size. The patterning processes yield particle arrays with well-defined geometrical shapes. As an example, in Fig. 1 a three-dimensional atomic-force microscopy (AFM) image of 10-nm-thick circular particles with $d_c=550$ nm is shown. Reference samples undergoing the same preparation processes as the particles were made of each of the Fe films. For magnetic measurements the wafers were diced into rectangular samples using a diamond saw.

Magnetic hysteresis curves were obtained with an alternating gradient magnetometer (AGM) from Princeton Measurements Corporation. The samples were investigated at room temperature with magnetic fields B in the range

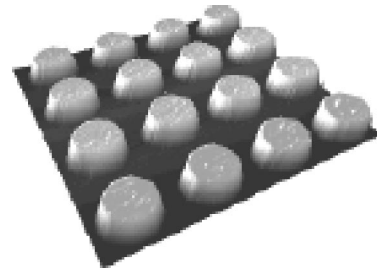


FIG. 1. An AFM image showing a three-dimensional (3D) view of the topography of circular Fe (001) particles with diameter 550 nm and thickness 10 nm. The scan area is 5×5 μm^2 .

$-2\text{ T} < B < 2\text{ T}$ applied in different directions in the plane of the film. The coercivity B_c and the saturation and remanent values of the magnetic moment, m_s and m_r , of the sample were determined from the hysteresis curves after correction for the diamagnetic background of sample holder and substrate. The values of m_s were found to be proportional to the amount of Fe in each sample, which implies that the intrinsic properties of the film are preserved and any oxidation of Fe during the preparation may be neglected. The saturation magnetization M_s and the saturation remanent magnetization M_r were obtained by dividing m_s and m_r by the volume of the magnetic material in each sample. The particle arrays were further investigated by MFM in a Dimension 3000 scanning probe microscope from Digital Instruments (DI). The tips were magnetized to obtain the main component of magnetization along the z axis, perpendicular to the plane of the samples. Magnetic images were obtained with the instrument operated in the tapping and lift mode using the standard MFM tips delivered by DI. The samples were investigated in the as-prepared state, in the remanent state after magnetization in an applied field, and in the state after ac demagnetization.

III. RESULTS

A. Fe films

The magnetic hysteresis curves of the reference films with the field applied in the $[110]$ direction are shown for fields in the ranges ± 0.2 T and ± 0.003 T in Fig. 2. The main shape of the curves shows the characteristics of magnetization along the intermediate direction in bulk Fe. In the curves there are three regimes related to different magnetization processes. Starting from saturation, during demagnetization the magnetization is constant until a field B_r is reached; see Fig. 2. Here the magnetic moments, initially aligned in the $[110]$ direction, start to rotate back to the easy $[100]$ direction. As the field is further decreased and reversed, nucleation of domain walls occurs at a field B_n (Fig. 2) and the magnetization switches direction. B_r and B_n are well defined by a kink that can be observed in the curves, except that of the 15-nm-thick film, which shows rather a continuous change in the slope of the magnetization versus field. The coercivity is low in all films, of the order of 0.5 mT; see Table I. A low coercivity is considered to indicate that the films are free of defects that would impede the movements of

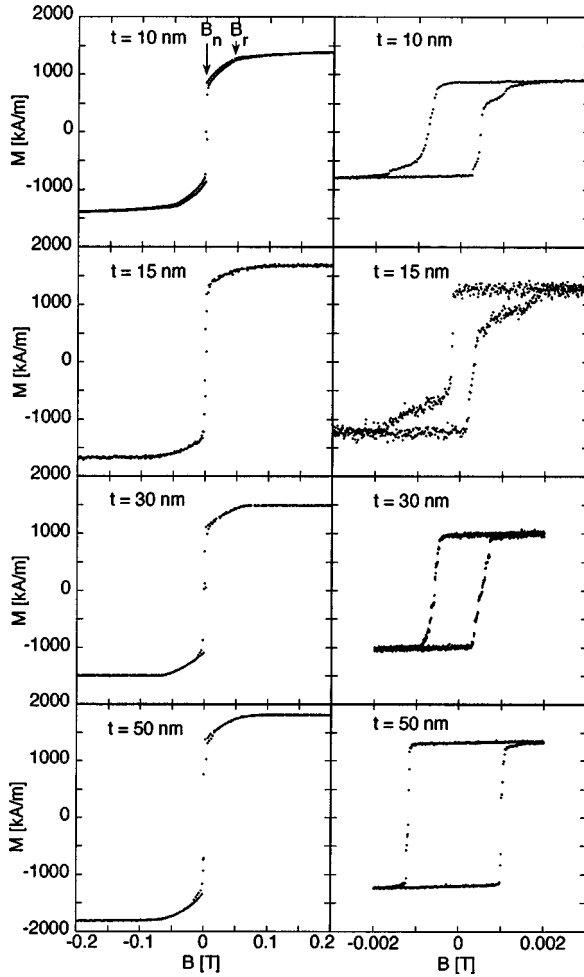


FIG. 2. The magnetization vs field of epitaxial Fe (001) films with thicknesses as indicated in the figure. The field was applied in the plane of the film along the [110] direction.

domain walls. However, in the low-field hysteresis curves (minor loops, Fig. 2, right column) showing the magnetization switching in more detail, one can see that whereas switching occurs mainly in one step in the 50- and 30-nm films, in the two thinner films the steep step is followed by an extended irreversible part before the magnetization loop is closed. This implies that in parts of these films domain walls are hindered to develop and move freely. The 15-nm film has the lowest coercivity, but a higher field is needed to close the hysteresis loop than in the thicker films. We attribute this difference to variations of the film properties due to imperfections in the MgO substrates¹⁶ for this particular film. The effects observed in the low-field hysteresis curve may also account for the rounding of the high-field hysteresis curve of the 15-nm-thick film. The relation between the remanent and the saturation magnetizations is $M_r \approx 0.7M_s$ for the three thickest films (see Table I), in good agreement with the ratio $1/\sqrt{2}$ expected when the saturation magnetization lying along the [100] direction is projected onto the [110] direction. For $t=10$ nm the ratio is slightly reduced: $M_r \approx 0.6M_s$. Such a thickness-dependent effect can be explained by the surface spins, which may be harder to align than the bulk of the film, comprising a proportionally larger part of the film as the

TABLE I. Magnetic parameters obtained from hysteresis curves of epitaxial Fe (001) films and particles of different thickness. The samples are Ref, reference samples; C, circular particles with the diameter given in nm; Rect, rectangular particles (300 nm by 900 nm); and Ell, elliptical particles (150 nm by 450 nm). The direction of the applied field is given with respect to a crystalline direction in Fe and along the long or short axis of the particles, respectively.

Sample	t (nm)	B along	B_c (mT)	M_r/M_s
Ref	30	[110]	0.6	0.71
Ref	20	[110]	0.3	0.75
Ref	10	[110]	0.6	0.56
C550	30	[100]	5.5	0.09
C550	30	[110]	0.5	0.02
C550	15	[100]	4.7	0.21
C550	15	[110]	5.0	0.25
C550	10	[100]	5.5	0.26
C550	10	[110]	5.5	0.26
C200	10	[110]	10.6	0.21
Rect	30	long	7.2	0.36
Rect	30	short	1.3	0.08
Rect	15	long	15.1	0.81
Rect	15	short	4.0	0.24
Rect	10	long	11.7	0.32
Rect	10	short	5.8	0.13
Ell	10	long	10.4	0.20
Ell	10	short	6.3	0.17

thickness decreases. We observed similar effects also in Co films.¹³ The first-order anisotropy constant K_1 estimated from the area between the hysteresis curves measured in the [100] and [110] directions yielded the room-temperature value⁶ $K_1 = 4.3 \times 10^4 \text{ J m}^{-3}$ for $t=50$ nm. For the thinner films the same kind of analysis yields $4.3 \times 10^4 \text{ J m}^{-3}$, $4.0 \times 10^4 \text{ J m}^{-3}$, and $5.7 \times 10^4 \text{ J m}^{-3}$ for $t=30, 15,$ and 10 nm, respectively. The estimated uncertainty in the values is $0.1 \times 10^4 \text{ J m}^{-3}$ for $t=10$ nm and somewhat less for the thicker films. The values of K_1 are in good agreement with the value for bulk iron, except for the 10-nm-thick film, yielding a significantly higher anisotropy constant. This is consistent with the findings that in thin films and small particles surface effects usually lead to an increase of the effective anisotropy. Thus, the magnetization measurements imply that the films are of good quality, with the crystalline structure as well as the orientation of the easy axes of magnetization in bcc Fe (001) remaining the same for all film thicknesses. Surface effects are evident in the remanent magnetization of the 10-nm-thick film.

B. Fe particles of circular shape

The magnetic hysteresis curves of the particles of circular shape with diameter 550 nm are shown for the field applied along the [100] and [110] directions in Fig. 3. The curves derived with the field applied parallel to the corresponding orthogonal directions in each sample are identical to the ones

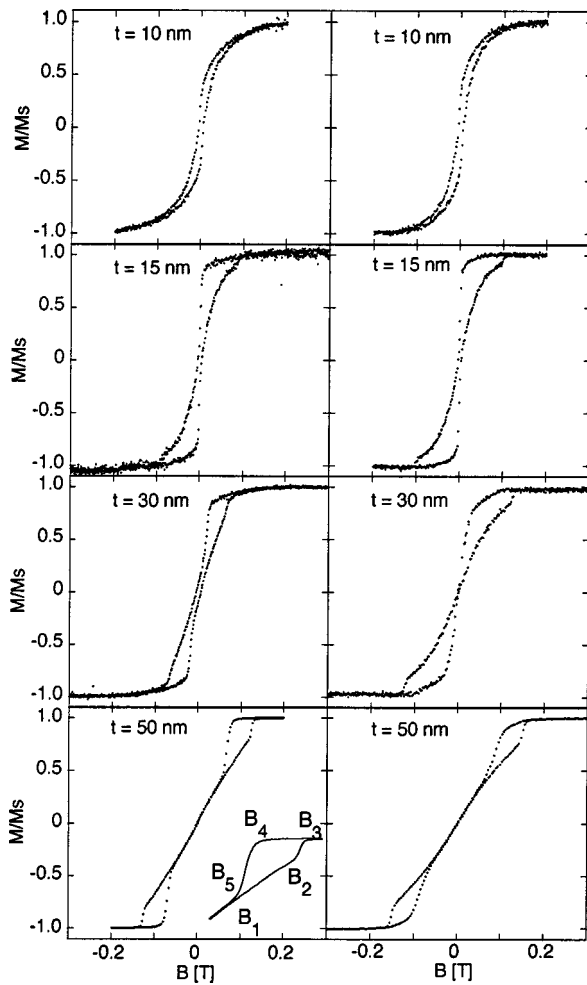


FIG. 3. The normalized magnetization vs field of circular particles with diameter 550 nm prepared from Fe (001) films of thicknesses as indicated in the figure. The field was applied in the plane of the film along the [100] and [110] directions in the left and right columns, respectively.

shown. In the overall behavior one can observe five different regions, indicated by the fields B_1 , B_2 , B_3 , B_4 , and B_5 in the magnetization curve for the 50-nm-thick particles; cf. the inset in Fig. 3. In the range from zero field up to B_1 the magnetization increases reversibly with applied field. As the film thickness decreases, the range of reversible magnetization becomes narrower and the hysteresis loop more open. The coercivity of the 50-nm-thick particles is the same as that of the corresponding film and the remanence is practically zero. As the film thickness decreases, the coercivity and remanence increase, yielding $B_c = 5.5$ mT and $M_r = 0.26M_s$ for the 10-nm-thick circular particles; see Table I. This coercivity is significantly increased as compared to the value $B_c = 0.6$ mT for the corresponding film. The shearing of the hysteresis loop shows that demagnetization effects are important in all samples. Furthermore, the initial slope increases in accordance with the decrease of the demagnetizing factors as the particle thickness is decreased while keeping the diameter constant. The demagnetization factors for the field applied in the easy direction obtained from the inverse of the initial slope of the hysteresis curves agree very well

with those calculated for generalized ellipsoids^{6,17} for the three samples with $d_c = 550$ nm, $t = 50$, 15, and 10 nm, yielding the values 0.06, 0.02, and 0.014, respectively. For $t = 30$ nm the experimental value is 0.03 and the calculated 0.04. This agreement is reasonable, considering that for this sample the uncertainty in the experimental value is larger than for the others, due to a shorter linear range of M versus B . The good agreement obtained when only demagnetization effects from individual particles were included implies that the influence of interactions between the particles is small. The interparticle interactions in a system of single-domain particles with the same geometrical dimensions would correspond to stray fields of order 2 mT, as estimated for a pair of magnetic dipoles. The interactions are considerably weaker for the particles with closed-domain structures, reduced by a factor 10^3 as estimated for a pair of interacting quadrupoles.

Above B_1 the magnetization increases slowly and irreversibly up to B_2 , where the slope increases, and finally the magnetization saturates at B_3 . For the samples with $t = 50$, 30, and 15 nm, where this field is well defined, the values obtained after correction for demagnetizing effects are equivalent to the fields required to saturate the corresponding Fe films. The demagnetization process is reversible until the field reaches B_4 . Then the magnetization decreases irreversibly until the demagnetization curve approaches the initial magnetization curve and the hysteresis loop is closed at $B_5 \approx B_1$. Such a magnetization curve is typical for noninteracting magnetic particles that are sufficiently large to accommodate domain walls. In zero field each particle comprises a multidomain state with zero remanence. The reversible parts of the magnetization curves are due to magnetization rotation and domain wall movements and the irreversible parts to annihilation, starting at B_2 , and nucleation, at B_4 , of domain walls. Whereas the annihilation as well as the nucleation of a domain wall in a single particle should occur in a sharp step, we observe the process to take place over a narrow field range. This can be explained by a distribution of annihilation

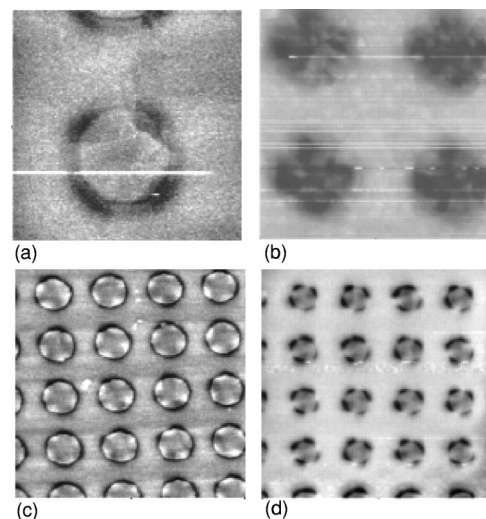


FIG. 4. MFM images of circular Fe (001) particles with diameter 550 nm and thicknesses: (a) 10 nm, (b) 15 nm, (c) 30 nm, and (d) 50 nm. The scan areas are (a) $1.5 \times 1.5 \mu\text{m}^2$, (b) $2 \times 2 \mu\text{m}^2$, and (c) and (d) $5 \times 5 \mu\text{m}^2$.

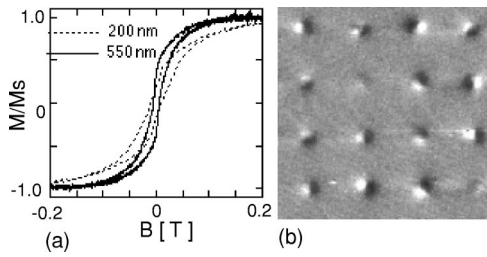


FIG. 5. (a) The normalized magnetization vs field applied in the [100] crystal direction of circular Fe (001) particles with thickness 10 nm and diameter 200 nm and 550 nm according to notations in the figure. (b) An MFM image of circular Fe (001) particles with diameter 200 nm and thickness 10 nm. The scan area is $5 \times 5 \mu\text{m}^2$.

and nucleation fields, among the 1.4×10^7 small particles comprising a sample. As the magnetization in a particle approaches saturation the interparticle interactions will increase and possibly also affect the switching properties of the particles. Comparing the magnetization along the two crystal-line directions one finds that the general behavior is the same, but a higher external field is required to annihilate the domain walls and nucleation starts earlier during the demagnetization process when the field is applied along the intermediate [110] than along the easy [100] direction. The hysteresis curves for the circular particles with $d_c = 550$ nm and $t = 10$ nm differ from the thicker ones in that there is a more gradual change of slope, and no distinct field values indicating the onset of different magnetization processes can be discerned. This can be explained by the surface effects and the strong effective anisotropy of the 10-nm-thick film.

The interpretation of the magnetization processes is supported by the magnetic domain structures observed in the MFM images; see Fig. 4. For all thicknesses, the images show a fourfold symmetry, being characteristic for a closed magnetic structure with the magnetization oriented along the [100] directions in the plane of the film. The particles with $t = 50$ and 30 nm are of great homogeneity throughout the samples. Among the thinner particles there are larger individual variations, and in addition to the four-fold symmetry, irregular domain walls can be observed in some of the particles, for instance the one shown in Fig. 4(a). When the diameter of the circular particles with $t = 10$ nm decreases to $d_c = 200$ nm, the particles become single domain. As can be seen in the MFM image, Fig. 5(b), each particle has a magnetic dipole moment with its orientation varying over the sample as a whole. The coercivity $B_c = 10.6$ mT is considerably lower than the switching field, $2K_1/M_s \approx 70$ mT, required for coherent rotation. Furthermore, the magnetization curves have the same characteristic features [Fig. 5(a)] as those with the same thickness and $d_c = 550$ nm. These results give evidence that for $d_c = 200$ nm the particle volume is small enough to comprise a single magnetic domain in zero field and yet magnetization reversal does not occur through coherent rotation.

C. Fe particles of rectangular and elliptical shape

The magnetic hysteresis curves obtained with the field applied parallel to the long and short axes of the particles of

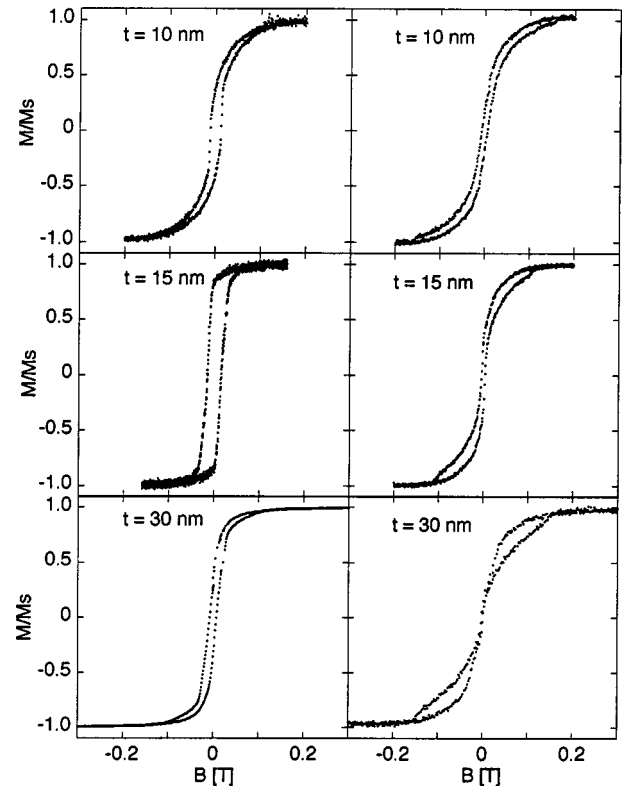


FIG. 6. The normalized magnetization vs field of rectangular Fe (001) particles with lateral size 900 nm by 300 nm and thicknesses as indicated in the figure. In the left column the field was applied along the long axis of the rectangles corresponding to the crystalline directions [100] for $t = 10$ nm, and [110] for 15 and 30 nm. In the right column the field was applied along the short axis corresponding to [010] for $t = 10$ nm and $[\bar{1}10]$ for 15 and 30 nm.

rectangular shape and $t = 30, 15,$ and 10 nm, are shown in Fig. 6. The coercivity of the particles is in all cases higher than that of the corresponding film and the influence of the shape anisotropy of the particles becomes evident from a comparison between the two directions of magnetization. When the field is applied along the short axis of the rectangles, the magnetization processes are very similar to those observed for the circular particles, but there is a significant difference when the field is applied along the long axis of the rectangles. For the particles with $t = 30$ and 15 nm the magnetization curve is more square, yielding higher coercivity and remanent magnetization; see Table I. The largest difference between the two directions is observed for the 15-nm-thick rectangles with $B_c = 15.1$ and 4.0 mT and $M_r/M_s = 0.81$ and 0.24 with the field applied along the long and short axes, respectively.

The MFM images of the rectangular particles in the demagnetized or as-prepared state (Fig. 7) show how the zero-field domain structures undergo a gradual change as the film thickness is decreased while the lateral dimensions of the particles are kept constant. The particles with $t = 50$ nm are divided into three closed magnetic substructures, having an internal rotation in a clockwise or anticlockwise direction, Fig. 7(d). When $t = 30$ nm the rectangles can accommodate two closed substructures, either having the same or opposite

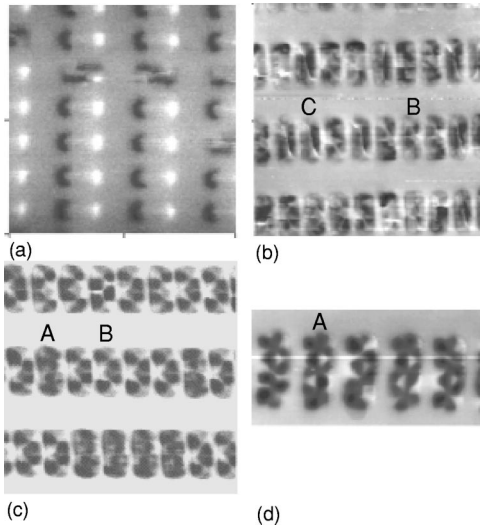


FIG. 7. MFM images of rectangular Fe (001) particles with lateral size 900 nm by 300 nm and thickness: (a) 10 nm, (b) 15 nm, (c) 30 nm, and (d) 50 nm. (a) shows the sample in the as-prepared state, which is identical to that after demagnetization. In (b)–(d) the samples were demagnetized in a field along the long axis of the particles. The scan areas are (a) $6 \times 6 \mu\text{m}^2$, (b) and (c) $5 \times 5 \mu\text{m}^2$, and (d) $5 \times 2.5 \mu\text{m}^2$. The scan direction is along the horizontal direction in each of the figures.

rotation directions, Fig. 7(c). The 15-nm-thick rectangles show a variety of domain structures. There are particles accommodating the same kind of two closed substructures as those with $t=30$ nm and others having two domains separated by a wall extending mainly diagonally across the rectangle, Fig. 7(b).

The 10-nm-thick rectangles, with axes along the [100] directions, are of great uniformity in the MFM images; see Fig. 7(a). The main structure is a dipole, with the magnetization direction along the long axis. A few of the particles were observed to change magnetization direction during the scan, due to the interaction with the MFM tip, as in the case of the particles with two dark and two bright areas in Fig. 7(a). The remanence of the particles magnetized along the long axis is low, $0.36M_s$ without and $0.50M_s$ with correction for demagnetizing effects in the individual particles, and decreased below that of the corresponding continuous film, being $0.65M_s$. Part of this reduction may be explained by the formation of end domains in the individual particles. When the moments of the particles are all aligned there may also be interactions between them, leading to additional macroscopic demagnetizing effects.

The elliptical particles ($d_s=150$ nm, $d_l=450$ nm, and $t=10$ nm) have the same aspect ratio and a volume reduced by about a factor of 4, as compared to that of the rectangles. The majority of these particles are stable single domains in zero field; i.e., they remain in this state also after demagnetization, Fig. 8(b). The low coercivity and shape of the magnetization curves, having the same character for magnetization along the long and short axes [Fig. 8(a)] and being similar to those of the particles described above, suggest that magnetization reversal does not occur by coherent rotation.

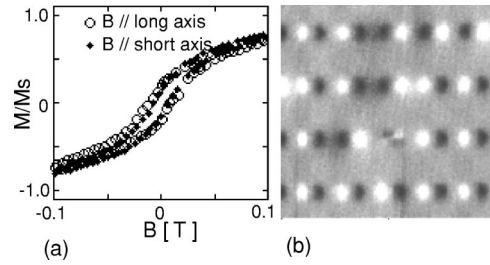


FIG. 8. Magnetic characteristics of elliptical Fe (001) particles with long and short axes 450 and 150 nm, respectively, and thickness 10 nm. (a) The normalized magnetization vs field. The field was applied, according to notations in the figure, along the long and short axes, corresponding to the [100] and [010] directions in Fe. (b) An MFM image obtained with a scan area $5 \times 5 \mu\text{m}^2$.

IV. DISCUSSION AND CONCLUSIONS

As shown by the magnetic measurements on the reference samples, we have grown Fe films with the same cubic anisotropy as that of bulk Fe for thicknesses 50, 30, and 15 nm. The 10-nm-thick film is more difficult to saturate, which we explain by the influence of surface effects. Effects of the interplay between magnetocrystalline and shape anisotropies, which occur when going from a continuous film to submicron-size particles, are clearly demonstrated in our experiments. It might be argued that the MFM images do not show the zero-field state of the magnetic particles, since they are affected by the stray fields from the magnetic tip. However, we consider the MFM images to represent stable zero-field states for the following reasons.

(i) The tip is magnetized to obtain a moment mainly in the z direction perpendicular to the plane of the film. The stray field from the tip, estimated to be of the order of $B_{tip} \approx 10$ mT, then should be compared to the coercivity (or rather switching field) of the particles when the field is applied perpendicularly to the plane of the film. The coercivities are generally substantially higher in this case than the values in Table I as observed for B applied in the plane of the film. The 10-nm-thick rectangles have a coercivity measured out of plane $B_c=14$ mT and, since they are thin, the stray field from the tip may be of the same magnitude throughout the particle. This can explain why some of these rectangles were observed to switch during scanning.

(ii) The character of the images remains the same independent of the lift scan height, i.e., the distance between the tip and sample during the scan that yields the magnetic image.

(iii) The symmetry of the domain structure is independent of scan direction. In particles of Permalloy, which is a soft material, one may observe an asymmetry in the patterns for different scan directions and domain walls may be seen to deform and move. Such effects were not observed in the Fe particles. Furthermore, the flux closed-domain structures observed in the MFM images are compatible with the low remanence obtained for a demagnetized sample.

(iv) We tried imaging with low-moment tips, which seem to yield the same patterns. The visibility was, however, not sufficient for presentation.

A. Fe particles of circular shape: Effects of decreased lateral extension

When the lateral dimensions of a ferromagnet are decreased one has to include a magnetostatic energy term E_{dem} in addition to the quantum mechanical exchange energy E_{exch} and magnetocrystalline anisotropy E_{anis} to obtain the total energy. With an external field H_{ext} applied, there will also be a Zeeman term E_{Zeem} . Numerical methods, so-called micromagnetic calculations, may be applied to find stable configurations of the direction of the magnetic moments. We used a public micromagnetics program¹⁸ OOMMF to simulate the zero-field magnetic domain structure in our particles. In the simulation the following numerical values were used: the exchange parameter $A = 21 \times 10^{-12} \text{ J m}^{-1}$, the saturation magnetization $M_s = 1.7 \times 10^6 \text{ A m}^{-1}$, and the anisotropy constant $K_1 = 4.3 \times 10^4 \text{ J m}^{-3}$. In order to obtain mesh independence¹⁹ the side of the square computational cells was chosen to be 3 nm or less. The results of the numerical calculation, displayed as vectors representing the in-plane projection of the pointwise magnetization, together with an MFM image of a circular Fe particle ($d_c = 550 \text{ nm}$ and $t = 50 \text{ nm}$) are shown in Fig. 9.

Although the present model and the MFM images may not be used for drawing conclusions about the spin arrangements on a microscopic scale, they explain well the character of the domain structures. In order to minimize the magnetostatic energy at a surface, the spins tend to align along the edges of the particles. In the interior the magnetostatic energy is less important, and the balance between exchange and magnetocrystalline anisotropy governs the behavior. In the case when the magnetocrystalline anisotropy energy is small, the exchange energy is minimized by making the angle between neighboring spins small. This is the case for isotropic Permalloy, where a gradual change of spin direction and contrast in the MFM image of particles of circular shape can be observed, shown, for instance, in Fig. 9(c) in Ref. 13. In Fe the crystalline anisotropy is strong enough to preserve the fourfold symmetry, with domains of spins aligned along the easy directions separated by regions of turning spins, domain walls. Thus, we have shown how a closed-domain structure develops when the lateral dimensions of the Fe film are decreased to 550 nm, without introducing any additional in-plane anisotropy. As the volume of the particles decreases, the gain in magnetostatic energy is less than the cost of cre-

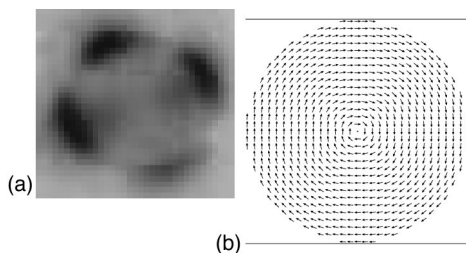


FIG. 9. The closed-magnetic-domain structure with fourfold symmetry of a circular particle of Fe (001) with diameter 550 nm and thickness 50 nm: (a) observed in an MFM image and (b) obtained from micromagnetic calculations.

ating domain walls, and the particles become single domains, as observed for the circular particles with $d_c = 200 \text{ nm}$ and $t = 10 \text{ nm}$.

B. Fe particles of rectangular and elliptical shape: Effects of shape anisotropy

There are two features to be observed when comparing the MFM images of the rectangular particles of different thicknesses: the number of closed substructures decreases and the lateral distribution of the contrast in the MFM images changes character as the film thickness decreases; see Fig. 7. The 50-nm-thick Fe particles of rectangular shape can be considered as the best representatives of samples in which the intrinsic bulk Fe properties are preserved. Furthermore, the edges of the particles are oriented along the easy [100] and [010] directions of magnetization, thus enhancing the alignment of spins into these directions. The domain structure can be simply described as comprising three closed substructures of quadratic shape; see particle (A) in Fig. 7(d), also shown in Fig. 10(b). In Fig. 10(a) the magnetization vectors obtained from the corresponding micromagnetic calculations are shown. This magnetization pattern has the same character as that calculated for particles of Permalloy-like materials, usually referred to as the diamond structure.¹⁹ The contrast of the MFM image has a dipolar character, with darker lobes separated by brighter spots. This feature is similar to that obtained from a simulation of the MFM contrast of four magnetic dipoles positioned in a square, with their moments oriented in the plane of the film forming a closed magnetic structure, Fig. 10(c). Furthermore, a model system having such a configuration of elliptical particles of Fe/Co multilayers was also observed to yield such an MFM contrast.²⁰ From these comparisons we conclude that the in-plane shape anisotropy of the rectangular particles causes a higher degree of spin alignment along the four easy directions as compared to the circular particles.

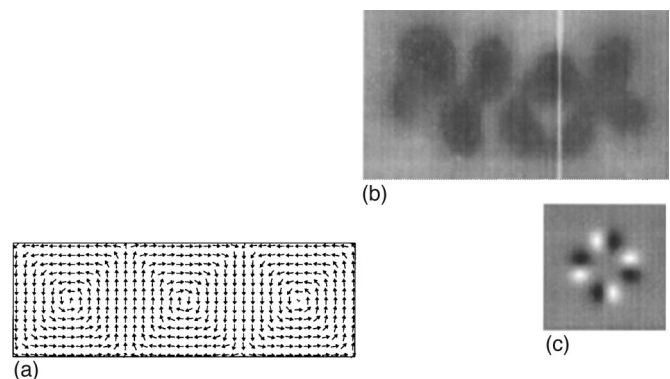


FIG. 10. The figure illustrates the MFM contrast and strong spin alignment, mainly caused by shape anisotropy. (a) Micromagnetic simulation of the spin orientation in a 50-nm-thick Fe (001) particle of rectangular shape (300 nm by 900 nm). (b) MFM image of the same particle. (c) Simulation of the MFM contrast obtained when a magnetic dipole oriented along the z direction is scanning the xy plane with four dipoles arranged in a square. This configuration corresponds to one of the three closed substructures in (b).

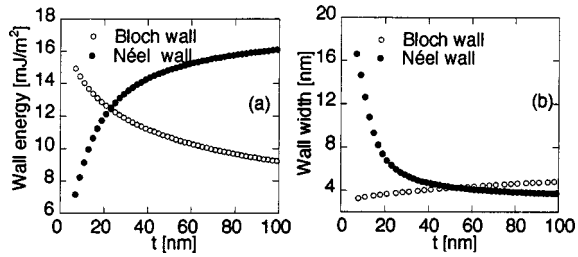


FIG. 11. (a) The wall energy and (b) the wall width vs film thickness for Bloch and Néel walls in Fe films with infinite lateral extension. The calculations were made adapting equations in Ref. 21.

The 30- and 15-nm-thick rectangular particles have their edges oriented along the $[110]$ and $[\bar{1}10]$ directions, which are the intermediate directions of magnetization in the crystal. The majority of the 30-nm-thick rectangular particles are divided into two equivalent rectangular substructures in their MFM images [Fig. 7(c)] among which we discern two different patterns (A) and (B). A few rectangles show the same fourfold dipolar character, state (A), as seen in the 50-nm-thick rectangles, Fig. 7(d). In others the fourfold symmetry is broken or, rather, superimposed by an additional twofold component, state (B). Also the 15-nm-thick rectangles have two main domain structures, one equivalent to state (B), Fig. 7(b), and another closed structure, state (C) in Fig. 7(b), comprising two main magnetic domains separated by a domain wall and with smaller end domains, where the moments adjust to the short sides of the rectangles.

We could not reproduce the observed thickness dependence with the OOMMF program. The reason for this may be that the thickness dependence of the domain walls is not properly taken into account. However, we suggest two physical phenomena offering an explanation of the change in domain structure: the transition from Bloch walls to Néel walls and the thickness dependence of the width of the walls. The transition from Bloch walls (spins rotating in the plane of the wall surface) to Néel walls (spins rotating in a plane parallel to the film) occurs at a thickness of order 10 nm in an Fe film with infinite lateral extension.¹⁷ One might assume that in a finite particle the transition takes place at thicknesses of the same order of magnitude. Then the 50-nm-thick rectangles may accommodate Bloch walls. These generate a considerable out-of-plane component in the field gradient, which leads to a strong contrast in the MFM images obtained with a scanning tip having its main magnetic component perpendicular to the film plane. As the film thickness decreases, the amount of Néel component in the walls will gradually increase. Then the out-of-plane component of the field gradient as well as the MFM contrast will decrease. The width of a Néel wall increases with decreasing film thickness, and becomes wider than the Bloch wall in the actual thickness range. We applied the equations in Ref. 21 to calculate the wall width and energy for Fe films; see Fig. 11. From these considerations it is reasonable to assume that it will be energetically favorable to decrease the total length of domain walls in accordance with the increasing wall width, by reducing the number of closed substructures in the particles. This is what we observe for the

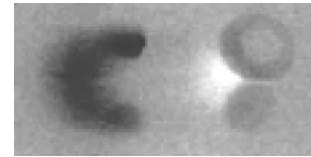


FIG. 12. MFM image of one of the 10-nm-thick Fe (001) particles of rectangular shape (300 nm by 900 nm) showing the quasisingle domain state. The main magnetization is directed along the long axis of the particle but diverges from a dipolar configuration at the corners.

rectangles in states (A) ($t=50$ and 30 nm), (B) ($t=30$ and 15 nm), and (C) ($t=15$ nm) with three, two, and one substructures, respectively. In state (C) the domain walls have become wide enough (of order 20–60 nm) to be clearly distinguished in the MFM image. The structure may be described as comprising two main magnetic domains separated by a 180° domain wall along a direction deviating from the $[110]$ towards $[100]$, which is the direction yielding the lowest wall energy in bulk Fe. At the short ends of the rectangles the spins gradually adjust along the edges.

For $t=10$ nm, finally, there are no longer any fully developed domain walls. The magnetization direction is mainly along the long axis of the rectangles. At the corners there is an enhancement of the field gradient, symmetric with respect to the long axis, implying a diverging magnetization with the spins aligning inwards from the corners in one of the short ends and outwards in the other, Fig. 12. This state has a character similar to what is called the flower state¹⁹ and may be referred to as being a quasisingle domain.

It is well known, from considerations of demagnetizing effects, that the magnetization can be homogeneous only in particles of ellipsoidal shape or elliptical in the case with the magnetization confined to the plane of a film. The influence of corners and the transition to a single-domain state can be readily observed when comparing the MFM images of rectangular [Fig. 7(a)] and elliptical [Fig. 8(b)] particles with the same aspect ratio. The influence of the edge shape on the switching properties, another important area of micromagnetics, can not be directly concluded from our experiments, since the actual particle volumes differ by about a factor of 4.

V. SUMMARY

In this work state-of-the-art methods were applied for preparing epitaxial Fe (001) films and arrays of submicron-size particles with well-defined geometry. The interactions between the particles are negligible and the magnetization curves and the variation between the samples can be explained by differences in demagnetization effects, angular orientation of the applied field with respect to the easy magnetization direction, and intrinsic film properties. The magnetic domain structure and magnetic hysteresis were investigated, and effects of the interplay between the magnetocrystalline and the shape anisotropies were clearly shown, as the lateral extension and thickness of the films were decreased. The following summarizes the main results.

(i) The cubic anisotropy of bcc Fe is preserved in the

films, yielding a first-order anisotropy constant $K_1 = (4.3 \pm 0.1) \times 10^4 \text{ J m}^{-3}$ for $t = 50, 30,$ and 15 nm . The effective anisotropy constant for $t = 10 \text{ nm}$ is increased to $K_1 = (5.7 \pm 0.1) \times 10^4 \text{ J m}^{-3}$, due to surface effects.

(ii) In the circular particles with diameter $d_c = 550 \text{ nm}$ the initial slope of the magnetization vs field, applied in the easy direction, increases with decreasing thickness in accordance with the demagnetizing factors determined from the particle shapes. The in-plane anisotropy is dominated by the magnetocrystalline component for all thicknesses. This leads to an ordering of the spins into zero-field domain states comprising closed structures of fourfold symmetry, with the spins aligned mainly along the crystalline easy directions of magnetization. Smaller circular particles, $d_c = 200 \text{ nm}$ and $t = 10 \text{ nm}$, were found to be stable single domains.

(ii) In rectangular particles, 300 nm by 900 nm , the domain structure undergoes a gradual change as the thickness decreases. For $t = 50 \text{ nm}$ three closed substructures are formed, with the spins aligned mainly along the easy crystalline directions and the particle edges, thus forming a diamond state. The number of substructures decreases with de-

creasing thickness, and for $t = 10 \text{ nm}$ a quasi-single-domain, flower, state is reached. The development of the domain structures and the character of the contrast in MFM images are explained by, in the actual thickness range, the domain walls undergoing a gradual transition from Bloch- to Néel-type walls with an accompanying thickness dependence of the wall widths. Elliptical particles with short and long axes 150 and 450 nm (the same aspect ratio as that of the rectangular ones) and $t = 10 \text{ nm}$ were found to be stable single domains.

ACKNOWLEDGMENTS

This work was financially supported by the Swedish Natural Science Research Council, the Swedish Research Council for Engineering Sciences, and SSF. We are grateful for a grant from the Royal Swedish Academy of Sciences. We also thank F. Eisele for help with the experiments. The sample patterning was performed at the Swedish Nanometer Laboratory at Chalmers University of Technology.

*Electronic address: maj.hanson@fy.chalmers.se

¹See, e.g., S.Y. Chou, Proc. IEEE **85**, 652 (1997).

²See, e.g., *The Physics of Ultra-High-Density Magnetic Recording*, edited by M.L. Plumer, J. van Ek, and D. Weller (Springer, Berlin, 2001).

³G. Prinz, Science **282**, 1660 (1998).

⁴S.A. Wolf, D.D. Awschalom, R.A. Buhrman, J.M. Daughton, S. von Molnar, M.L. Roukes, A.Y. Chtchelkanova, and D.M. Treger, Science **294**, 1488 (2001).

⁵S. Kreuzer, K. Prügl, G. Bayreuther, and D. Weiss, Thin Solid Films **318**, 219 (1998).

⁶M. Hanson, C. Johansson, B. Nilsson, P. Isberg, and R. Wäppling, J. Appl. Phys. **85**, 2793 (1999).

⁷O. Fruchart, W. Wernsdorfer, J.-P. Nozières, D. Givord, F. Rousseaux, D. Maily, D. Decanini, and F. Carcenac, J. Magn. Magn. Mater. **198-199**, 228 (1999).

⁸J.-E. Wegrove, O. Fruchart, J.-P. Nozières, D. Givord, F. Rousseaux, D. Decanini, and J.Ph. Ansermet, J. Appl. Phys. **86**, 1028 (1999).

⁹Y.B. Xu, A. Hirohata, L. Lopez-Diaz, H.T. Leung, M. Tseleoi, S.M. Gardiner, W.Y. Lee, J.A.C. Bland, F. Rousseaux, E. Cambril, and H. Launois, J. Appl. Phys. **87**, 7019 (2000).

¹⁰Y. Otani, T. Kohda, S.G. Kim, K. Fukamichi, O. Kitakami, and Y.

Shimada, J. Magn. Magn. Mater. **198-199**, 483 (1999).

¹¹M. Demand, M. Hehn, K. Ounadjela, R.L. Stamps, E. Cambril, A. Cornette, and F. Rousseaux, J. Appl. Phys. **87**, 5111 (2000).

¹²J. Rothman, M. Klaui, L. Lopez-Diaz, C.A.F. Vaz, A. Bleloch, J.A.C. Bland, Z. Cui, and R. Speaks, Phys. Rev. Lett. **86**, 1098 (2001).

¹³O. Kazakova, M. Hanson, P. Blomqvist, and R. Wäppling, J. Appl. Phys. **90**, 2440 (2001).

¹⁴M. Hanson, C. Johansson, B. Nilsson, and E.B. Svedberg, J. Magn. Magn. Mater. **236**, 139 (2001).

¹⁵P. Isberg, E.B. Svedberg, B. Hjörvarsson, R. Wäppling, and L. Hultman, Vacuum **48**, 483 (1997).

¹⁶L.D. Madsen, R. Charavel, J. Birch, and E.B. Svedberg, J. Cryst. Growth **209**, 91 (2000).

¹⁷S. Chikazumi, *Physics of Magnetism* (Wiley, New York, 1964).

¹⁸The Object Oriented MicroMagnetic Framework project at ITL/NIST <http://math.nist.gov/oommf/> access date October 23, 2001.

¹⁹W. Rave and A. Hubert, IEEE Trans. Magn. **36**, 3886 (2000) and references therein.

²⁰M. Hanson, O. Kazakova, P. Blomqvist, and R. Wäppling, J. Appl. Phys. **91**, 7044 (2002).

²¹A. Aharoni, *Introduction to the Theory of Ferromagnetism* (Clarendon Press, Oxford, 1996).